http://dx.doi.org/10.5012/bkcs.2014.35.6.1832

A Deep Investigation of the Thermal Decomposition Process of Supported Silver Catalysts

Jun Jiang,[†,‡] Tianhao Xu,[†] Yaping Li,[†] Xiaodong Lei,[†] Hui Zhang,[†] D. G. Evans,[†] Xiaoming Sun,[†,*] and Xue Duan[†]

[†]*State Key Laboratory of Chemical Resource Engineering, Beijing University of Chemical Technology, Beijing 100029, P.R. China.* [*]*E-mail: sunxm@mail.buct.edu.cn*
[‡]*Beijing Research Institute of Chemical Industry, Beijing 100013, P.R. China*
Received January 4, 2014, Accepted March 2, 2014

A deep understanding of the metallic silver catalysts formation process on oxide support and the formation mechanism is of great scientific and practical meaning for exploring better catalyst preparing procedures. Herein the thermal decomposition process of supported silver catalyst with silver oxalate as the silver precursor in the presence of ethylenediamine and ethanolamine is carefully investigated by employing a variety of characterization techniques including thermal analysis, *in situ* diffuse reflectance infrared Fourier transform spectroscopy, scanning electron microscopy, and X-ray diffraction. The formation mechanism of supported silver particles was revealed. Results showed that formation of metallic silver begins at about 100 °C and activation process is essentially complete below 145 °C. Formation of silver was accompanied by decomposition of oxalate group and removal of organic amines. Catalytic performance tests using the epoxidation of ethylene as a probe reaction showed that rapid activation (for 5 minutes) at a relatively low temperature (170 °C) afforded materials with optimum catalytic performance, since higher activation temperatures and/or longer activation times resulted in sintering of the silver particles.

Key Words : Silver, Supported catalyst, Thermal decomposition, Activation, Epoxidation

Introduction

Ethylene epoxidation is one of the most important reactions in the petrochemical industry.[1-3] Silver is commonly employed as the catalyst and its performance depends on both particle size and crystal facets exposed.[4-6] By controlled synthesis in solution, colloidal silver nanocubes and nanowires with mostly (100) exposed facets have been obtained which has shown excellent selectivity.[6,7] Pioneering work by Li's group is especially instructive[7] and scaled-up production of such shape-controlled catalysts tightly bound to a catalyst support remained a challenge to realize. It is more realistic to improve the conventional silver catalyst preparation method.

Conventional commercial silver catalysts are α-Al_2O_3 supported metallic silver usually prepared by the impregnation–calcination method. From previous studies it is clear that properties of the final catalysts are significantly dependent on both the silver precursor and the preparation method employed.[8,9] Metallic silver catalysts can be prepared by reduction of a variety of precursors including its oxide,[10-12] nitrate,[9,13] oxalate,[14,15] lactate,[16] and other salts (*e.g.* silver neodecanoate[12]). Silver oxalate is a particularly attractive precursor for large-scale production of silver catalysts as it can be dissolved in organic amines giving solutions with a concentration as high as 30 wt % (based on Ag).[8] In commercial catalyst production with silver oxalate as silver precursor, calcination is used to form supported metallic silver nanoparticles, which is a thermal decomposition (activation) process. So far little study on the thermal decomposition process was publicly and deeply reported. A deeper understanding of the metallic silver catalysts formation process on oxide support and the formation mechanism would be of great scientific and practical meaning for further exploring better catalyst preparing procedures. In this work, we deeply studied the thermal decomposition process of alumina-supported silver oxalate in the presence of ethylenediamine and ethanolamine in an attempt to reveal the formation mechanism of supported silver particles and further optimized the silver catalyst preparation method. It is found that the thermal decomposition took place rapidly in range of 100–145 °C, and heating at 170 °C for 5 min was sufficient for complete activation. Use of such relatively low temperatures and short activation times favors the formation of small nanometer silver particles with high catalytic activity in the epoxidation of ethylene.

Experimental

Preparation of the Silver Catalysts. Silver catalysts are prepared by an incipient wetness procedure. Silver oxalate is dissolved in an aqueous mixture containing 22.6 wt % ethylenediamine and 7.6 wt % ethanolamine giving a solution containing 22 wt % silver. α-Al_2O_3 (with a specific surface area and pore volume of 1.0 m^2/g and 0.50 mL/g respectively) is impregnated with the solution under vacuum. The impregnated material is heated (activated) at different temperatures such as 140, 170, 250, 300 or 350 °C for 5 minutes, or at 350 °C for 10 and 20 minutes, or at 210 °C for 30 minutes in air on a belt roaster. As-prepared samples are

denoted Act140, Act170, A250, Act300, Act350, Act350-10, Act350-20, and Act210-30 respectively.

Analysis and Characterization. Thermogravimetry and differential scanning calorimetry (TG-DSC) analysis were carried out with a NETZSCH STA-449C thermal analysis instrument with a heating rate of 10 °C/min and an air flow of 100 mL/min. Temperature-programmed desorption–mass spectrometry measurements (TPD–MS) were conducted at a heating rate of 10 °C/min in air to monitor the decomposition products when activating the impregnated sample. A HPR 20QIC mass spectrometer was used to monitor gaseous products evolved in the course of heating. The carbon dioxide produced was monitored at m/e = 44.

In situ diffuse reflectance infrared Fourier transform spectra (DRIFTS) were collected on a Bio-Rad FTS-135 spectrometer. The background spectrum was first recorded, then the sample was sequentially heated to 50, 80, 120, 160, 200, 300 and 420 °C, and after stabilizing at the required temperature for two minutes, the IR spectra were recorded. IR spectra of the sample at different temperatures were obtained by difference spectrum treatment.

A Hitachi S-4700 scanning electron microscope (SEM) was used to examine the silver particle size and morphology. Based on the SEM images, the average silver particle size and its standard deviation was measured and calculated for each sample.

XRD patterns of the catalysts activated at different temperatures were acquired on a Rigaku D/Max 2500 powder X-ray diffractometer (XRD) using Cu Kα radiation at 40 kV and 40 mA.

Catalytic Performance Testing. A fixed-bed tubular quartz reactor was used to measure the catalytic performance of the samples. Silver catalysts were crushed and sieved. About 0.2 g of sample with particle size of 12–30 mesh was diluted with quartz sand (the weight ratio of catalyst:quartz was 1:2). Catalytic performance was determined initially under the standard reaction conditions (at 190 °C and 0.16 MPa, with a flow rate of 100 mL/min of a reaction feed containing 13% ethylene and 7% oxygen with the balance being nitrogen). After stabilizing (typically 3–20 h) under the required reaction conditions, the gas composition of the reactor gas effluent was analyzed and quantified using an on-line gas chromatograph (GC2014) equipped with a thermal conductivity detector (TCD) and a HP-PLOT Q capillary column. Reaction was also carried out at reaction temperatures of 180 and 170 °C, with the other conditions remaining unchanged. Based on the gas composition, ethylene conversion (Conversion) and selectivity to ethylene oxide (S_{EO}) are calculated as follows:

$$\text{Conversion} = \frac{\text{EO(outlet)} + 0.5\text{CO}_2\text{(outlet)}}{\text{ET(inlet)}} \times 100\% \quad (1)$$

$$S_{EO} = \frac{\text{EO(outlet)}}{\text{EO(outlet)} + 0.5\text{CO}_2\text{(outlet)}} \times 100\% \quad (2)$$

where EO(outlet), CO_2(outlet) and ET(inlet) respectively refer to the volumetric contents of ethylene oxide (EO) and CO_2 in the effluent gas and that of ethylene(ET) in the feed.

Results and Discussion

In order to investigate the formation of the supported metallic silver catalyst in air, thermal analysis was performed to simulate the thermal decomposition process. Figures 1(a) and 1(b) show the thermogravimetric (TG) and differential scanning calorimetry (DSC) results.

According to the TG curve (Figure 1(a)), the activation process can be divided into three stages: (1) from room temperature to ~100 °C, which can be attributed to solvent removal; (2) 100–145 °C, which can be attributed to decomposition of the catalyst precursor and release of gaseous products; and (3) > 145 °C, involving the sintering and

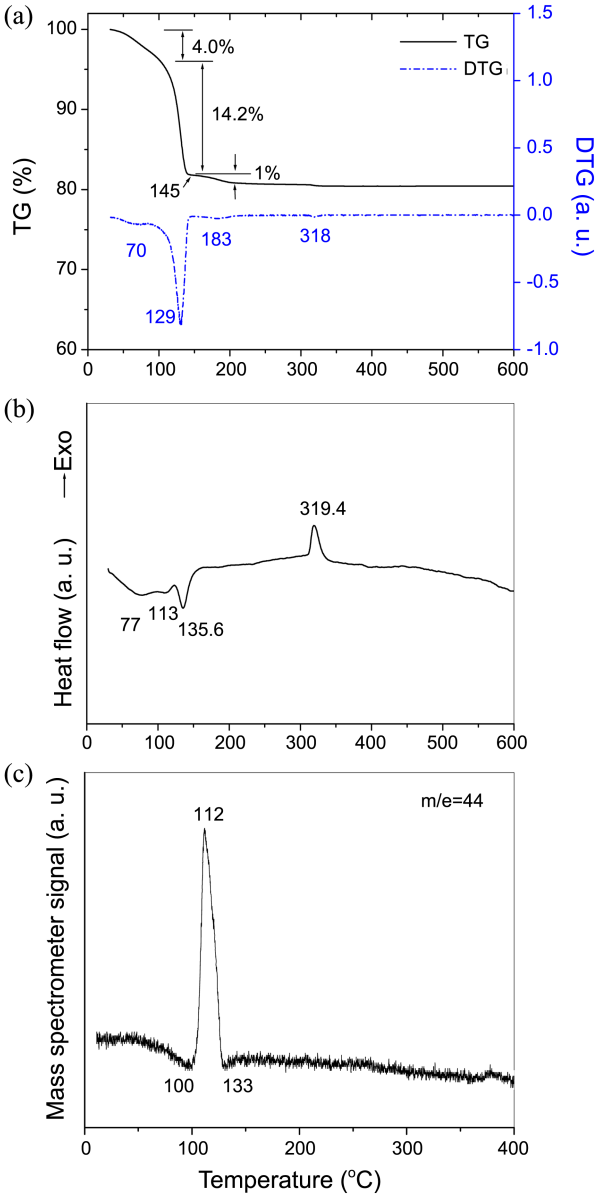

Figure 1. Thermal analysis curves and TPD results of the impregnated sample; (a) TG–DTG curve, (b) DSC curve, and (c) TPD spectrum for CO_2 (m/e = 44) released from the impregnated sample.

fusion of silver particles, which releases the residual gaseous products. The weight loss in the second stage (100–145 °C) was the most significant, as confirmed by the differential thermogravimetric curve (DTG), where the peak at 129 °C is much larger than the other three peaks (at 70, 183 and 318 °C). In the third stage of TG curve (above 145 °C), there was only a very small weight loss of about 1%. The DSC curve (Figure 1(b)) showed three endothermic peaks at 77, 113, and 135.6 °C and an exothermic peak at 319.4 °C. The endothermic changes are associated with the decomposition process, whilst the peak at 319.4 °C in the DSC curve (with a corresponding peak at 318 °C in DTG curve) can be attributed to the combustion of a trace amount of a carbonaceous residue.

The TPD–MS data in Figure 1(c) show that carbon dioxide was produced when the impregnated sample was heated in the range 100–133 °C, confirming that the oxalate decomposed in the second stage in the TG curve with concomitant formation of metallic silver.

In situ diffuse reflectance IR Fourier transform spectroscopy (DRIFTS) was utilized to investigate the evolution of the Ag catalyst during activation (Figure 2). The IR absorption bands in the initial spectrum of the material heated at 50 °C can be assigned to N–H stretching vibrations (3245 and 3134 cm^{-1}), $–CH_2–$ stretching vibrations (2920 and 2850 cm^{-1}), $–CH_2–$ deformation vibrations (1460 and 1350 cm^{-1}), –OH deformation vibrations (1298 cm^{-1}), C–N stretching vibrations (1100 and 1040 cm^{-1}). The additional broad IR absorption band at about 1600 cm^{-1} can be attributed to the N–H deformation vibration of amines and the C=O stretching vibration of oxalate. The broad band between 2000 cm^{-1} and 3650 cm^{-1} is consistent with the presence of water. The negative peaks at 2360 and 2340 cm^{-1} arise from carbon dioxide in the background spectrum.

Heating the sample resulted in changes in the number and intensity of vibrational bands. In the spectrum recorded at 80 °C, the organic amine bands became more obvious, which can be attributed to the evaporation of water and the resulting increase in surface amine concentration on the catalyst support. However the amine peak intensities decreased dramatically when the temperature was increased to 120 °C. The marked decrease in the intensity of the band at 1600 cm^{-1} can be attributed to both loss of amines and decomposition of oxalate moieties. A band at 1686 cm^{-1} emerged during the heating process, which can be assigned to an amide carbonyl group, suggesting a side reaction occurs during thermal decomposition. On heating the sample to 160 °C, the bands ascribed to organic amines almost disappeared completely and the band at 1686 cm^{-1} became more obvious, confirming that an amide compound was generated by partial oxidation of the amines. The band at about 1600 cm^{-1} disappeared completely at the same time, suggesting that the oxalate groups had decomposed completely, consistent with the formation of carbon dioxide observed in the TPD curve (Figure 1(c)) of the second decomposition stage. When the temperature was elevated above 300 °C, all the bands from the amines and oxalate disappeared completely, confirming

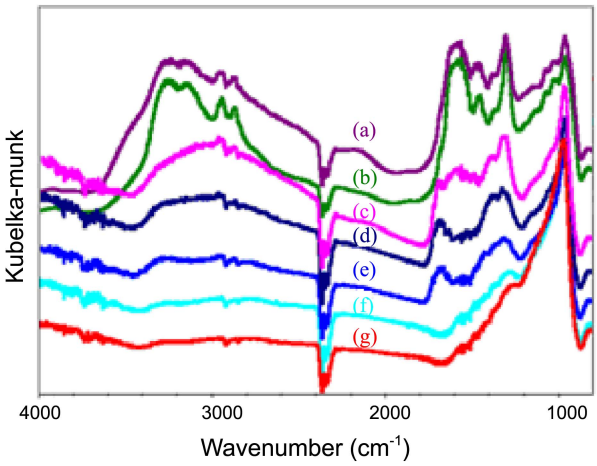

Figure 2. *In situ* DRIFTS spectra of the sample recorded at different temperatures; (a) 50 °C, (b) 80 °C, (c) 120 °C, (d) 160 °C, (e) 200 °C, (f) 300 °C, and (g) 420 °C.

the complete removal of organic compounds from the alumina support. The loss of the IR band at 1686 cm^{-1} can be attributed to the combustion of the amide compound, consistent with the exothermic peak at 319.4 °C observed in the DSC curve and the weight loss peak at 318 °C in the DTG curve.

In order to characterize the products formed between 100 °C and 145 °C, X-ray diffraction and scanning electron microscopy were used to examine the samples activated at different temperatures for 5 minutes; the results are shown in Figure 3 and Figure 4, respectively.

It can be seen that generation of silver particles starts after activating the sample at 140 °C for 5 min (Figure 3(a)), but the silver particles were extremely small (Figure 4(a)). In addition to the characteristic peaks of metallic silver and the α-alumina support, there were some other peaks in the diffraction pattern of Act140. These peaks are indicative of the formation of an intermediate species since these disappeared from the diffraction pattern of the material activated at 170 °C (as shown in Figure 4(b)), suggesting the comple-

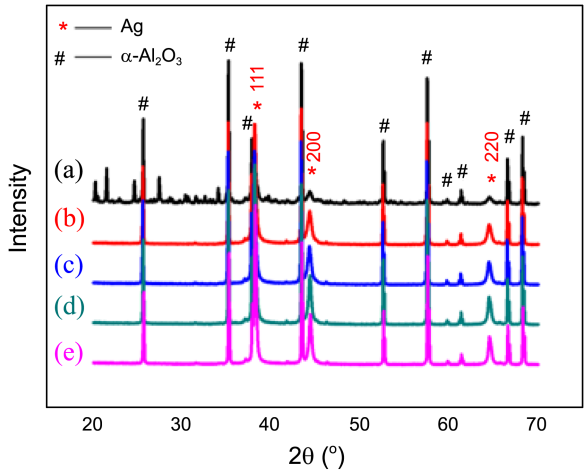

Figure 3. X-ray diffraction patterns of the catalysts; (a) Act140, (b) Act170, (c) Act250, (d) Act300, and (e) Act350.

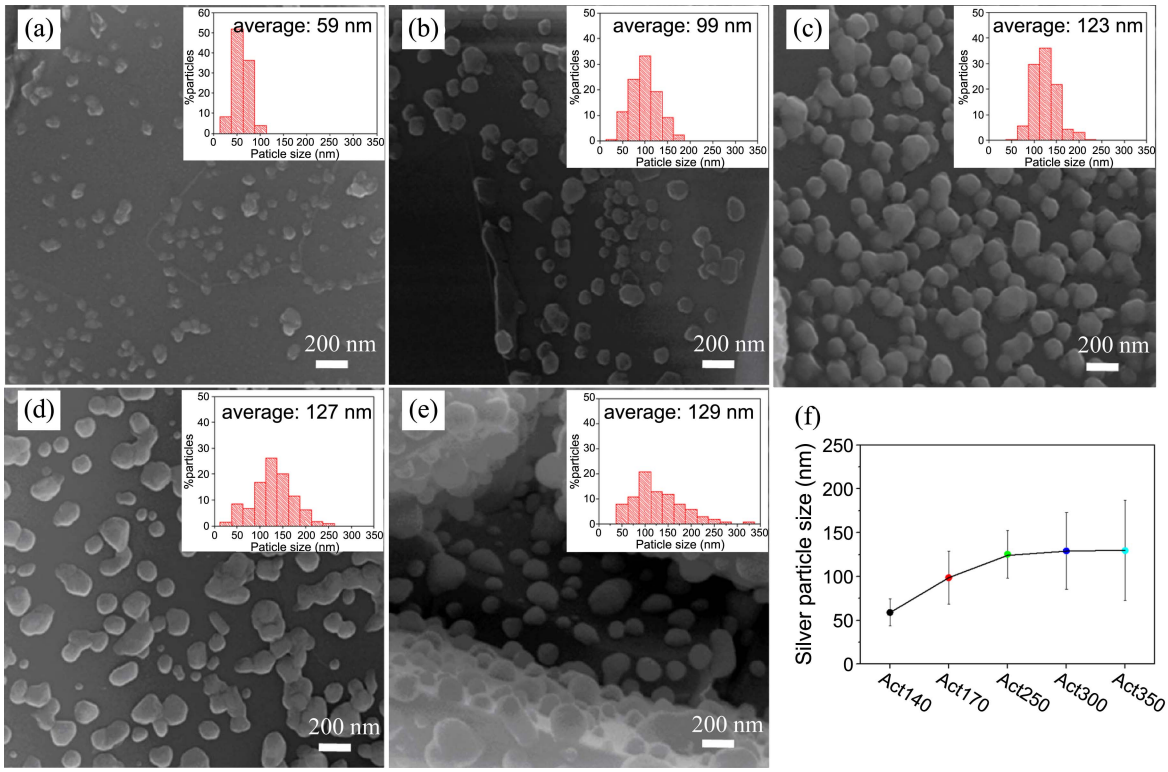

Figure 4. SEM images and silver particle size distribution in the catalysts; (a) Act140, (b) Act170, (c) Act250, (d) Act300, (e) Act350, and (f) average size distribution and its standard deviation for silver particles in the catalysts.

tion of conversion to silver at this temperature. This is consistent with the TG curve in Figure 1, which showed that the activation was essentially complete at about 145 °C. On heating above 170 °C (Figures 3(c)–3(e)), diffraction peaks of silver became sharper and more intense, indicating sintering of silver particles, but there was no additional changes in the diffraction patterns. The data therefore suggest that complete activation of the silver catalyst can be achieved by heating at 170 °C for 5 min.

The average size and size distribution of the silver particles were determined from SEM images (Figures 4(a)–4(e)). The average size of the silver particles increased as the activation temperature was raised from 140 to 250 °C, but the increase in average size on heating above 250 °C was negligible. However statistical analysis of the results (Figure 4(f)) showed that the standard deviation in average particle size increases with increasing activation temperature, showing that the width of the silver particle size distribution increases with activation temperature, consistent with the sintering of catalyst particles at relatively high temperatures.

Catalytic performance of the samples for epoxidation of ethylene were compared using a micro-reactor and are shown in Figure 5. It was found that in each case the catalytic activity decreased with increasing activation temperature, while the selectivity remained almost unaffected (Figure 5(a)). The sample activated at 170 °C showed the highest catalytic activity and smallest size of silver particles (samples activated at lower temperatures were not evaluated, since the characterization data discussed above indicate that these contain some carbonaceous materials). Effect of activation time was also examined and the results are shown in Figure 5(b). The results demonstrated that prolonging activation time resulted in lower catalytic activation. The catalyst Act210-30, which was activated for a longer time, had a lower activity and selectivity than Act350, further suggesting that short activation times favor high catalytic activity. Though results from thermal analysis suggests that 13 minutes are sufficient to complete activation of the catalyst at 145 °C, the optimum catalyst is obtained by heating at a

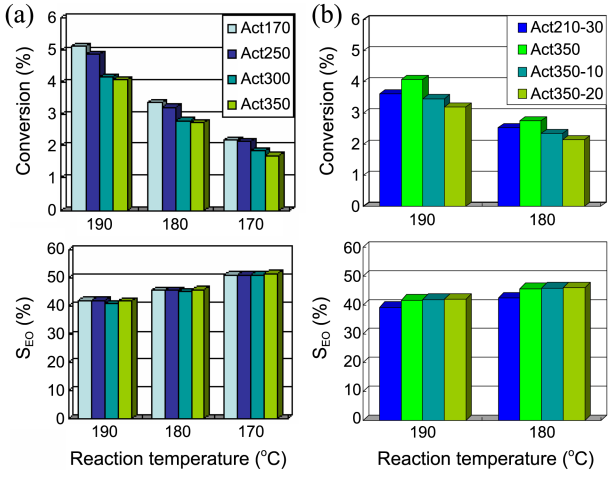

Figure 5. Catalytic performance of catalysts activated at different conditions: effects of activation temperature (a) and activation time (b) on catalytic performance.

slightly higher temperature (170 ºC) for a shorter time (5 min). Activation at higher temperatures and/or for longer times has an adverse effect on catalytic activity, because sintering of silver crystals results in larger particle sizes and a wider particle size distribution, with a corresponding reduction in the active surface area of the silver catalyst.

Conclusion

The formation process of silver catalysts by thermal decomposition of alumina-supported silver oxalate in the presence of ethylenediamine and ethanolamine was carefully investigated and results indicated that it involves a rapid endothermic process. The loss of amines and decomposition of oxalate moieties mainly take place between 100 to 145 ºC, and are accompanied by the formation of silver particles. Although the activation is essentially complete on prolonged heating below 145 ºC, the optimum catalytic activity can be obtained by activating silver catalyst by heating at a slightly higher temperature (170 ºC) for a shorter time (5 min). Whereas, activation at higher temperatures and/or for longer times results in sintering of silver particles and has an adverse effect on catalytic activity.

References

1. Denton, D.; Falling, S.; Monnier, J.; Stavinoha, J.; Watkins, W. *Chim. Oggi /Chem. Today* **1996**, *14*, 17.
2. Grasselli, R. K.; Burrington, J. D. *Adv. Catal.* **1981**, *30*, 133.
3. Peschel, A.; Karst, F.; Freund, H.; Sundmacher, K. *Chem. Eng. Sci.* **2011**, *66*, 6453.
4. Wu, J. C.; Harriot, P. J. *Catal.* **1975**, *39*, 395.
5. Goncharova, S. N.; Paukshtis, E. A.; Bal'zhinimaev, B. S. *Appl. Catal. A: Gen.* **1995**, *126*, 67.
6. Christopher, P.; Linic, S. *ChemCatChem.* **2010**, *2*, 78.
7. Xu, R.; Wang, D. S.; Zhang, J. T.; Li, Y. D. *Chem. Asian J.* **2006**, *1*, 888.
8. Hassani, S. S.; Ghasemi, M. R.; Rashidzadeh, M.; Sobat, Z. *Crystal Res. Tech.* **2009**, *44*, 948.
9. Dellamorte, J. C.; Lauterbach, J.; Barteau, M. A. *Top. Catal.* **2010**, *53*, 13.
10. Bhasin, M. M. U.S. Patent 5,057,481, 1988.
11. Rizkalla, N.; Klein, R.; Milne, S. B. U.S. Patent 5,854,167, 1997.
12. Becker, M.; Liu, K. H. U.S. Patent 4,663,303, 1986.
13. Kemp, R. A. U.S. Patent 5,545,603, 1994.
14. Buffum, J. E.; Kowaleski, R. M.; Gerdes, W. H. U.S. Patent 5,145,824, 1991.
15. Masahide, S.; Hitoshi, T. U.S. Patent 6,153,556, 1998.
16. Armstrong, W. D. U.S. Patent 4,760,042, 1988.